ELSEVIER

Strain and stress field in Taiwan oblique convergent system: constraints from GPS observation and tectonic data

Chung-Pai Chang [a,*], Tsui-Yu Chang [b], Jacques Angelier [c], Honn Kao [d], Jian-Cheng Lee [d], Shui-Beih Yu [d]

[a] *Center for Space and Remote Sensing Research, National Central University, Chungli 320, Taiwan*
[b] *Institute of Geophysics, National Central University, Chungli 320, Taiwan*
[c] *Laboratoire de Tectonique, Université P. et M. Curie, 4 place Jussieu, 75252 Paris Cedex 05, France*
[d] *Institute of Earth Sciences, Academia Sinica, P.O. Box 1-55, Nankang, Taipei 115, Taiwan*

Abstract

This paper focuses on the stress and strain rate field of the Taiwan area. The strain rate field in the Taiwan region is studied qualitatively and quantitatively, based on the GPS observation in 1990–1995. It reflects the accommodation of the ongoing lithospheric deformation within the seismogenic portion of lithosphere and exhibits zones with contrasting deformation modes and amounts. We then compare the obtained strain rate field with the tectonic information provided by studies of borehole breakouts and earthquake focal mechanisms for the Present, and by fault slip data analyses for the Quaternary period. In the first approximation, the stress and strain rate fields show spatial similarity. The orientation of principal shortening is generally consistent with the compressive stress orientation that reflects the oblique indentation of the Luzon Arc into the Eurasian continental margin. In more detail, significant anomalies in the deformation pattern deserve consideration in that they may reveal ongoing stress accumulation. Despite the short-term variations related to the earthquake cycle, some major features of the strain rate field, including the distribution of extension and compression, highlight the long-term tectonic behavior of the mountain belt at the lithospheric scale. The time and space variations of strain should be a function of local heterogeneity and be transferred between interseismic and coseismic periods.
© 2003 Elsevier B.V. All rights reserved.

Keywords: strain; stress; GPS; Taiwan

1. Introduction

The island of Taiwan is a product of the oblique collision between the Luzon arc and the Chinese continental margin (Fig. 1). The present-day collision process in Taiwan is vigorous, as revealed by the high seismic activity [1,2], the rapid contraction [3], and mountain building-related uplift [4]. The deformations in the Taiwan convergent system have been largely studied based on a variety of geological and geophysical observations. Some authors have suggested that the deformation in Taiwan is a simple physical con-

* Corresponding author. Tel.: +886-3-422-7151 ext. 7627; Fax: +886-3-425-4908.
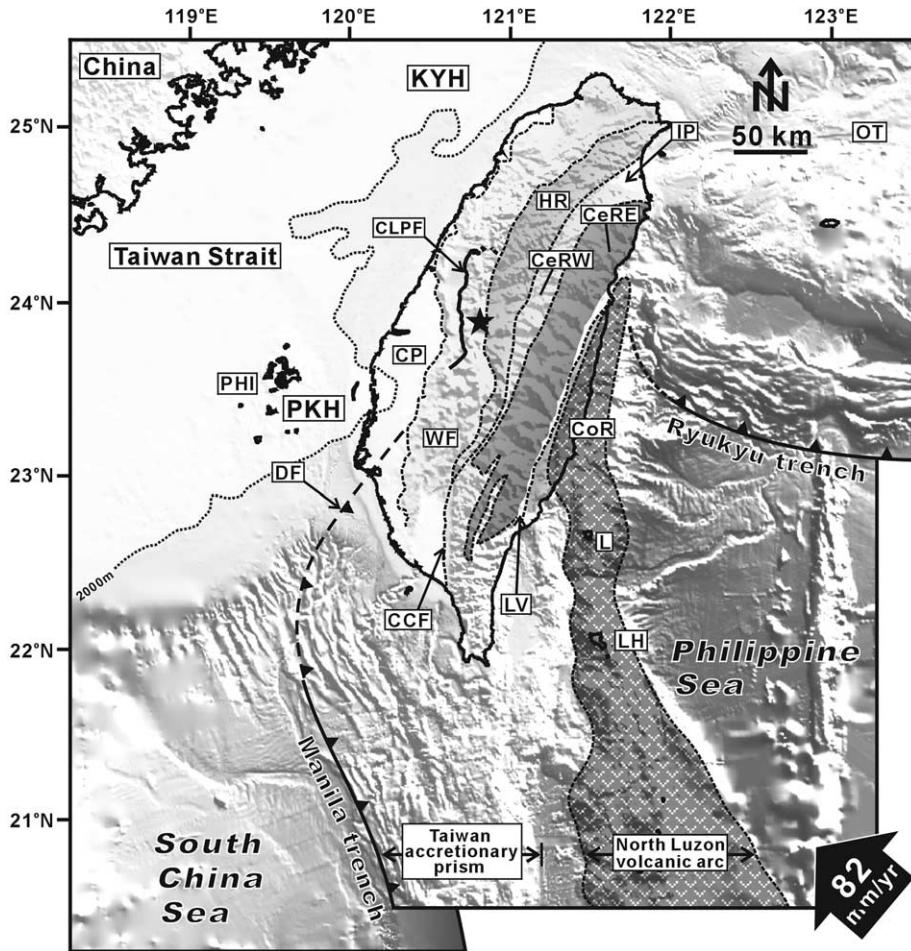*E-mail address:* cpchang@csrsr.ncu.edu.tw (C.-P. Chang).

Fig. 1. Geodynamic framework around Taiwan. The DEM (Taiwan Digital Bathymetry Model) used in this figure is after National Center for Ocean Research, Taiwan. Displacement of the Philippines Sea plate relative to southeast Eurasia is indicated by the large black arrow at the right-lower corner with velocity according to GPS studies [3]. Thick solid lines indicate subduction boundaries with the triangle on overriding side. Black star: Epicenter of Chi-Chi earthquake. Abbreviated terms of tectonic units: CCF, Chaochu Fault; CeRE, eastern Central Range; CeRW, western Central Range; CLPF, Chelungpu fault (main surface rupture of the Chi-Chi earthquake); CoR, Coastal Range; CP, Coastal plain; DF, deformation front; HR, Hsüehshan Range; IP, Ilan plain; KYH, Kuanyin High; L, Lutao; LH, Lanhsu; LV, Longitudinal Valley; PHI, Penghu island; PHK, Pei-kang High; WF, Western Foothill.

sequence of plate convergence, within the frame of a unique system from eastern collision to westward propagation of stress and strain (e.g. [5,6]). To some extent, numerical models of stress–strain relationships throughout Taiwan have supported such views [7]. In this paper, we do not aim at addressing such general aspects of Taiwan geodynamics. Instead, we analyze the type, amplitude and distribution of the present-day deformation throughout the Taiwan island. It is worth noting

that this deformation is far from being homogeneous, or even continuous.

We take advantage of the numerous relative displacement data issued from the 'Taiwan GPS Network' established in 1989 by the Institute of Earth Sciences, Academia Sinica. The results of GPS surveys for the whole island from 1990 to 1995 (Fig. 2) were published in 1997 [3]. Although it is conceivable that crustal deformation processes are too complex to be defined by a single meth-

od of observation, the GPS geodetic surveys provide the most accurate information about the present-day movement. It should be noted, however, that the data considered herein do not include the coseismic deformation related to major earthquakes of Taiwan like the Chi-Chi earthquake, which occurred in central Taiwan with moment magnitude 7.6 on 20 September 1999 (Fig. 1). These data rather illustrate the rate of deformation of the interseismic period. Concerning the coseismic deformation related to the destructive Chi-Chi earthquake, the reader can be referred to the studies on coseismic accelerometric record and GPS surveys (e.g. [8–10]).

Our aim is two-fold: we first reconstruct a refined strain rate field of Taiwan based on the GPS measurements. We then compare this strain rate field with the tectonic information provided by studies of borehole breakouts and earthquake focal mechanisms for the Present, and by fault slip data analyses for the Quaternary period. Our goal, therefore, is to evaluate the degree of consistency between the independent reconstructions of the present-day and recent tectonic patterns in Taiwan.

2. Geological background

The island of Taiwan is located at the junction between two subduction systems. East of Taiwan, the Philippine Sea plate (PH) subducts northward beneath the Eurasian plate (EU) along the Ryukyu subduction system. South of Taiwan, the Philippine Sea plate overrides the crust of the South China Sea at the Manila trench, which extends northward from the Philippines to a latitude of about 21.5°N (Fig. 1). In the Taiwan area, the convergent rate between the northern Luzon volcanic arc, which is located on the Philippine Sea plate, and the southeast Eurasian continental margin is about 8.2 cm/yr in the azimuth of 310° as determined by the GPS observations [3] (Fig. 2). This rate is about 15% faster than that of the PH–EU relative motion predicted from global plate models [11,12].

The general structural trends of the Taiwan mountain belt show an elongate S-shape (Fig. 1). The presence of two major basement highs on the Eurasian plate, the Kuanyin High to the north and the Peikang High to the south, is consistent with this particular shape because it resulted in the indentation of the foreland fold-and-thrust belt. These basement highs originated from the continental lithosphere experiencing normal faulting prior to collision, and show in situ tectonic stability, in strong contrast with the adjacent mobile belt [13,14].

As a result of regional compression, the Taiwan island consists of several provinces [15] with a main structural grain that trends NNE (Fig. 1). From west to east, they are: the Penghu island group, the Coastal Plain, the Western Foothills, the Hsüehshan Range, the Central Range, the Longitudinal Valley, and the Coastal Range. The Penghu island group in the Taiwan Strait is covered with Pleistocene flood basalt. The Coastal Plain, Western Foothills and Hsüehshan Range are composed of thick sequences of Cenozoic shallow-marine siliciclastics. These sequences are deformed by a combination of folds and thrust faults, which trend mainly northeast or north and dip toward the east or southeast [15,16]. The Central Range is divided into two parts. The western flank is underlain by weakly metamorphosed Cenozoic argillite–slate series, while the eastern flank is composed of the pre-Tertiary basement complex affected by Neogene greenschist facies and higher grades of polyphase Mesozoic–Cenozoic metamorphism.

Although significant convergence occurs at the front of the mobile mountain belt, the Longitudinal Valley (LV in Fig. 1), the suture zone between the eastern Central Range and the Coastal Range is also one of the most active deformation zones in Taiwan [2,3]. The straight and narrow Longitudinal Valley is bounded at the east by the Longitudinal Valley Fault (LVF). This LVF is a very active thrust with left-lateral strike-slip component (e.g. [17–19]). East of the LVF, the Coastal Range is mainly composed of Neogene andesitic volcanic units and associated flyschoid and turbidite sediments. Whereas the geological provinces west of the Longitudinal Valley originated as part of the underthrust Eurasian continent, the Coastal Range belongs to the Philippine Sea plate [15]
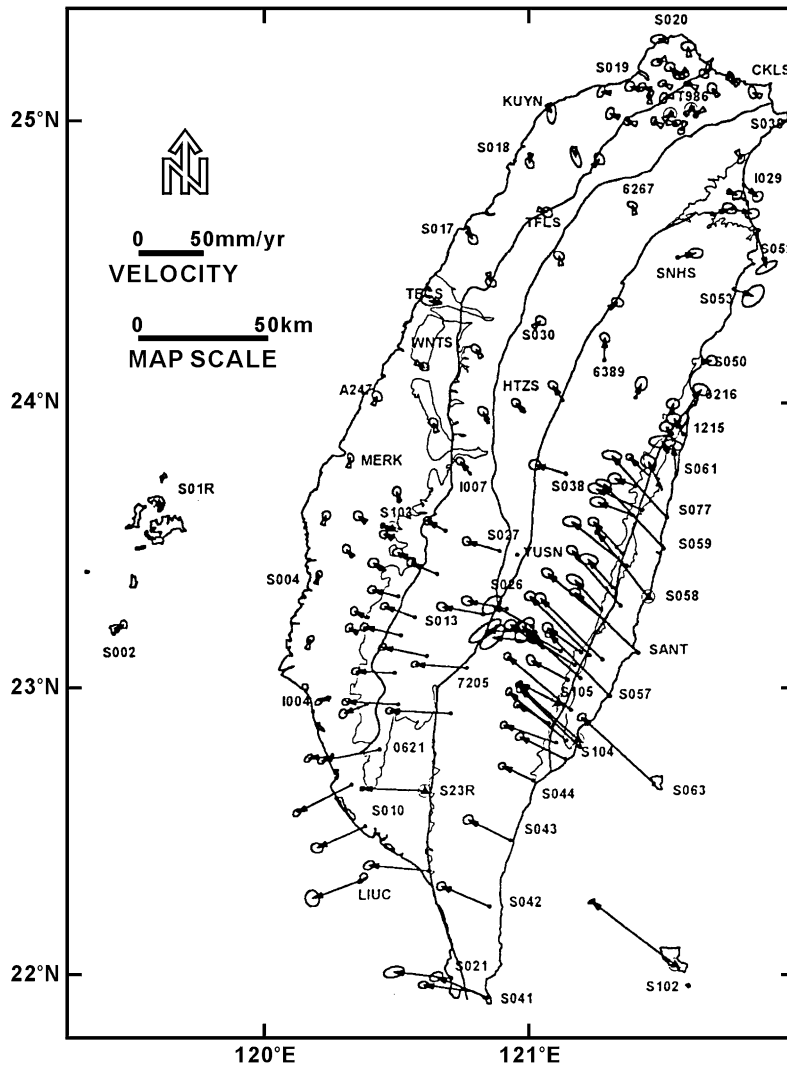
Fig. 2. Horizontal displacement rate, assumed to be steady in a period of 5 years (1990–1995), measured with 131 mobile and nine permanent GPS stations (after [3]). The 95% confidence interval of the error ellipse is shown at the tip of each velocity vector.

and represents a section of the Luzon arc that is being accreted onto the Eurasian continent (Fig. 1).

3. The 1990–1995 strain field of Taiwan

3.1. Data and analysis

The Taiwan GPS Network is composed of 131 annually surveyed mobile stations and nine permanent or semi-permanent continuously recording stations. The relative displacement data used in this study were collected during 5 years (1990–1995). Within this network the variations in baseline length show a generally constant rate [3]. All available temporary and continuous GPS data were processed with the Bernese GPS software v.3.4 (Astronomical Institute of the University of Berne, Switzerland). The average rates of

length change between nearby stations are determined by linear regression in time domain. The individual values of the average length are weighted by the reciprocal square of the standard error in the rate. Ultimately, $\vec{d}_{EW}$ and $\vec{d}_{NS}$ are the derived velocity measures in east and north directions, with positive values representing the eastward and northward motions, respectively (Fig. 3a). The observed horizontal velocity field in Taiwan (Fig. 2) shows a fan-shaped pattern. There is no need to discuss in detail the GPS data processing, which has been thoroughly described elsewhere [3]. We rather emphasize below the principle and results of our analysis.

The main goal of this study is to characterize a continuous deformation field of Taiwan through the determination of local two-dimensional surface strain rate tensors in the horizontal plane, inside a square-based grid. As the GPS measures are irregularly distributed in geography, it was necessary to re-calculate the velocity at each node of the grid, using a linear interpolation algorithm (Fig. 3b). The algorithm involves adjustable tension with continuous curvature, in order to prevent undesired oscillation and occurrence of false local maxima and minima [20]. This interpolation process puts strong emphasis on the nearby measurement point as compared with distant ones, which allows better characterization of local variations in the rate of deformation field. In our study, the gridding interpolation was implemented from 120°E to 122°E in longitude and 21.5°N to 25.5°N in latitude (Fig. 4). The interval was chosen as small as possible (0.1° on the sphere, that is, about 11 km), within realistic bounds that depend on the density of the GPS network. It should be noted that highly localized deformation related to short active faults cannot generally be reconstituted based on the scattered GPS data points because the station spacing is large. A remarkable exception, however, is that of the Longitudinal Valley in eastern Taiwan, where the narrow E–W spacing of many stations allows better resolution than our grid spacing permits ([3]; see Fig. 2).

The strain rate tensor of unit area is determined by spatial derivatives of velocity measurement in the N–S and E–W directions, as mentioned above.
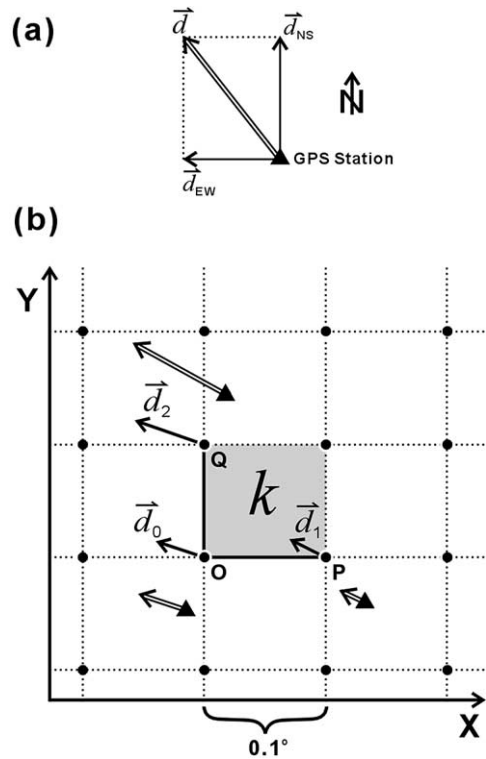

Fig. 3. Schematic diagram showing the measured components and our geometrical approach. (a) $\vec{d}_{EW}$ and $\vec{d}_{NS}$ are the measured vectors from one GPS station; $\vec{d}$ is the resulting vector. (b) Deformation of a small square in the horizontal plane, named unit k. k is bounded with corners at points O, P, and Q which are placed to new positions according to the velocity vectors $\vec{d}_0$, $\vec{d}_1$, and $\vec{d}_2$, respectively. The deviations among these three displacement vectors define the deformation of unit k.

Remembering that the velocity data used in this study deal with the average ground movement in a period of 5 years without significant coseismic movement, we consider that the ground surface is subject to deformation. This assumption implies that even where velocity discontinuities are present (e.g. fault creep) we determine the equivalent average deformation rate within each square mesh. Because the meshes are small with respect to the size of the whole studied area, the possibility to characterize the deformation related to large shear zones is maintained. Under this assumption of continuously distributed deformation, we can define mathematical functions for strain as the continuous spatial derivatives.

Fig. 3b presents the scheme of velocity of a small unit. For block κ, the strain rate tensor is derived from three displacement vectors that correspond to the mean motions previously calculated at nodes O, P and Q (SW, SE and NW mesh corners, respectively). The three displacement vectors are noted as follows:

$$\vec{d_i} = \vec{u_i} + \vec{v_i} \tag{1}$$

where $\vec{u_i}$, $\vec{v_i}$ are the velocities measured along the Cartesian axes X and Y (east and north directions, respectively), $\vec{d_i}$ is the motion vector at corner i, i ($i = 0, 1, 2$) being the index defined according to the scheme of Fig. 3b. Except in particular cases (e.g. three identical velocity vectors implying block translation without deformation), each block k is subject to two-dimensional simple shear and pure shear in variable proportions. The deformation rate of the block is derived from the displacement deviations with respect to a reference vector, which by convention is that of the SW corner of the space unit, $\vec{d_0}$. The normal strains are thus defined as:

$$\begin{cases} \varepsilon_{xx} = \dfrac{\partial \vec{u}}{\partial x} = \dfrac{\vec{u_1} - \vec{u_0}}{\Delta x} \\ \varepsilon_{yy} = \dfrac{\partial \vec{v}}{\partial y} = \dfrac{\vec{u_2} - \vec{v_0}}{\Delta y} \end{cases} \tag{2}$$

Accordingly, the shear strains are:

$$\begin{cases} \varepsilon_{xy} = \dfrac{1}{2}\left(\dfrac{\partial \vec{u}}{\partial y} + \dfrac{\partial \vec{v}}{\partial x}\right) = \dfrac{1}{2}\left(\dfrac{\vec{u_2} - \vec{u_0}}{\Delta y} + \dfrac{\vec{v_1} - \vec{v_0}}{\Delta x}\right) \\ \varepsilon_{yx} = \dfrac{1}{2}\left(\dfrac{\partial \vec{v}}{\partial x} + \dfrac{\partial \vec{u}}{\partial y}\right) = \dfrac{1}{2}\left(\dfrac{\vec{v_1} - \vec{v_0}}{\Delta x} + \dfrac{\vec{u_2} - \vec{u_0}}{\Delta y}\right) \end{cases} \tag{3}$$

Note that $\varepsilon_{xy} = \varepsilon_{yx}$. These four terms, given by Eqs. 2 and 3, constitute the strain rate tensor of the block k, a symmetric tensor with three independent quantities expressed as the following strain tensor matrix:

$$\varepsilon_k = \begin{bmatrix} \dfrac{\partial \vec{u}}{\partial x} & \dfrac{1}{2}\left(\dfrac{\partial \vec{u}}{\partial y} + \dfrac{\partial \vec{v}}{\partial x}\right) \\ \dfrac{1}{2}\left(\dfrac{\partial \vec{v}}{\partial x} + \dfrac{\partial \vec{u}}{\partial y}\right) & \dfrac{\partial \vec{v}}{\partial y} \end{bmatrix} \tag{4}$$

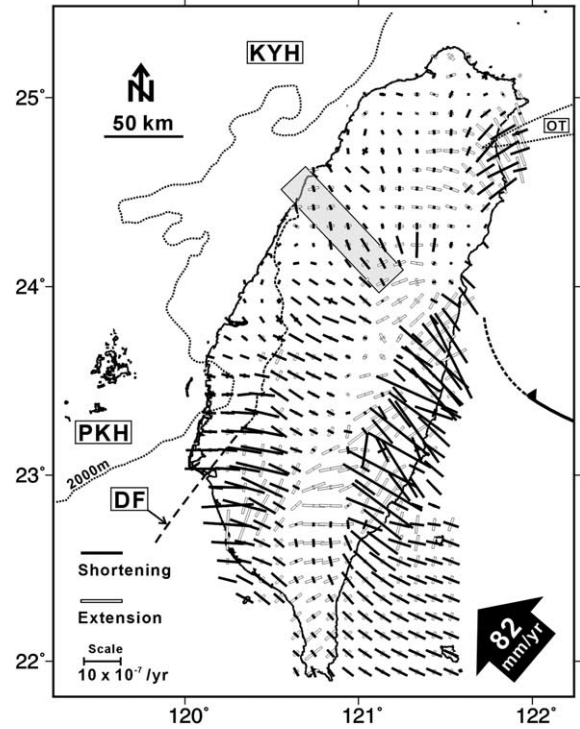Two eigenvalues are determined as the roots of

Fig. 4. Resultant strain rate field of Taiwan. Bars indicate eigenvectors and eigenvalues of the horizontal deformation field. Solid bars refer to shortening, and open bars refer to extension. The strain pairs derived from the extrapolation outside of the GPS network are faded. The gray rectangular zone in central Taiwan indicates the NW–SE trending Sanyi–Puli seismicity zone. PKH, Peikang High; KYH, Kuanyin High; OT, Okinawa Trough; DF, deformation front.

Eq. 5, where λ is the scaling constant of Eq. 5, while **I** refers to the identity matrix. The same equation is used to determine the corresponding two eigenvectors:

$$|\varepsilon_k - \lambda \mathbf{I}| = 0 \tag{5}$$

The resultant eigenvalues and eigenvectors derived from each unit block can therefore compose the strain rate field for the Taiwan region, whose features are introduced in the following context.

3.2. Resultant strain rate field

Fig. 4 shows the strain rate field derived from the 1990–1995 average motion surveyed by the

Taiwan GPS network. At each node, two perpendicular bars indicate the orientations and amounts of principal strain in the horizontal plane; the black solid bar represents shortening deformation, whereas the open bar corresponds to extensional deformation. The bar length is proportional to the strain rate magnitude.

At the first approximation, the strain rate of Taiwan presents a fan-shaped distribution, especially for the north and west. In more detail, the spatial variation of the resultant strain rates reflects the heterogeneity of local geology. The maximum deformation occurs in eastern Taiwan, in the Longitudinal Valley (Fig. 4), where the maximum shortening orientation approximately corresponds to the collision direction, well documented from previous studies (e.g. [3,11,12]). This is consistent with the high-angle reverse faulting with left component that actively occurs along the Longitudinal Valley [17,18]. Further to the northeast, the Ilan plane also reveals a high strain rate, but consistent with its extensional behavior related to the Okinawa Trough opening (e.g. [21, 22]).

In western Taiwan, the Peikang High, an east-northeast trending horst composed of continental crust, appears to separate the compressive deformation pattern of the foreland belt in two parts, with very small rates to the north and higher rates to the south (Fig. 4). The orientations of deformation in the north and south of the Peikang High also slightly differ in types of both compressive and extensional strain (Fig. 4). In the northern part, lots of the resultant strain rate patterns exhibit compressive deformation in two strain axes (Fig. 4), while one remarkable feature in the middle of this northern part (gray zone in Fig. 4) is a strike-slip mode of deformation shown at the location consistent with the Sanyi–Puli seismic zone, which is reported as a transfer fault zone that constrained the structural development of central Taiwan [23].

To the south of the Peikang High, the large strain magnitudes and the strike-slip and even extensional nature of the deformation are presented (Fig. 4). The direction of extension is generally from central Taiwan to the southwest, which is quite different with that in the Central Range.

This feature may be constrained by the tectonic partition of a large N–S trending fault, for example the activity of the Chaochu Fault (see location in Fig. 1), and can review the southwestward escape process reported in this area [24,25].

4. Recent and present-day stress field of Taiwan

To understand the tectonic activity in the Taiwan mountain belt, one should also take into account the stress data, which refer to the most recent step in the geodynamic evolution of the collision zone (Fig. 5). The present-day and recent distribution of tectonic stress in Taiwan discussed below was obtained from three principal sources of data: borehole breakout analyses, earthquake focal mechanism analyses and stress inversions of fault slip data collected in the field.

The map of maximum compressive stress trends obtained from borehole breakout data provides insights into the stress state in the uppermost crust of Taiwan [26]. The bars shown in Fig. 5a describe the inferred trends of the maximum compressive stress in the horizontal plane, σ_{hmax}, as revealed by borehole breakout experiments in the Taiwan area. Because the deformation is generally corresponding to strike-slip faulting or reverse faulting in western Taiwan, one of the principal stress axes, σ_2 or σ_3, should be vertical or nearly vertical, and the axis of maximum compressive stress (σ_1) is generally near-horizontal. As a consequence, the direction of σ_{hmax} derived from the borehole breakout data approximately corresponds to the direction of σ_1 in this area. The map of Fig. 5a shows that in western Taiwan the compression trends NW on average.

In 1992, the Institute of Earth Sciences, Academia Sinica, initiated the Broadband Array in Taiwan for Seismology (BATS). At present, broadband waveforms are retrieved from BATS stations on a regular basis, resulting in the determination of earthquake focal mechanisms. The description of the inversion algorithm is given in previous studies [27,28]. We summarize the results from 1995 to 2000 in Fig. 5b,c. The focal depth of earthquakes used in this study is less than 25 km, so that all the results refer to upper crustal levels.
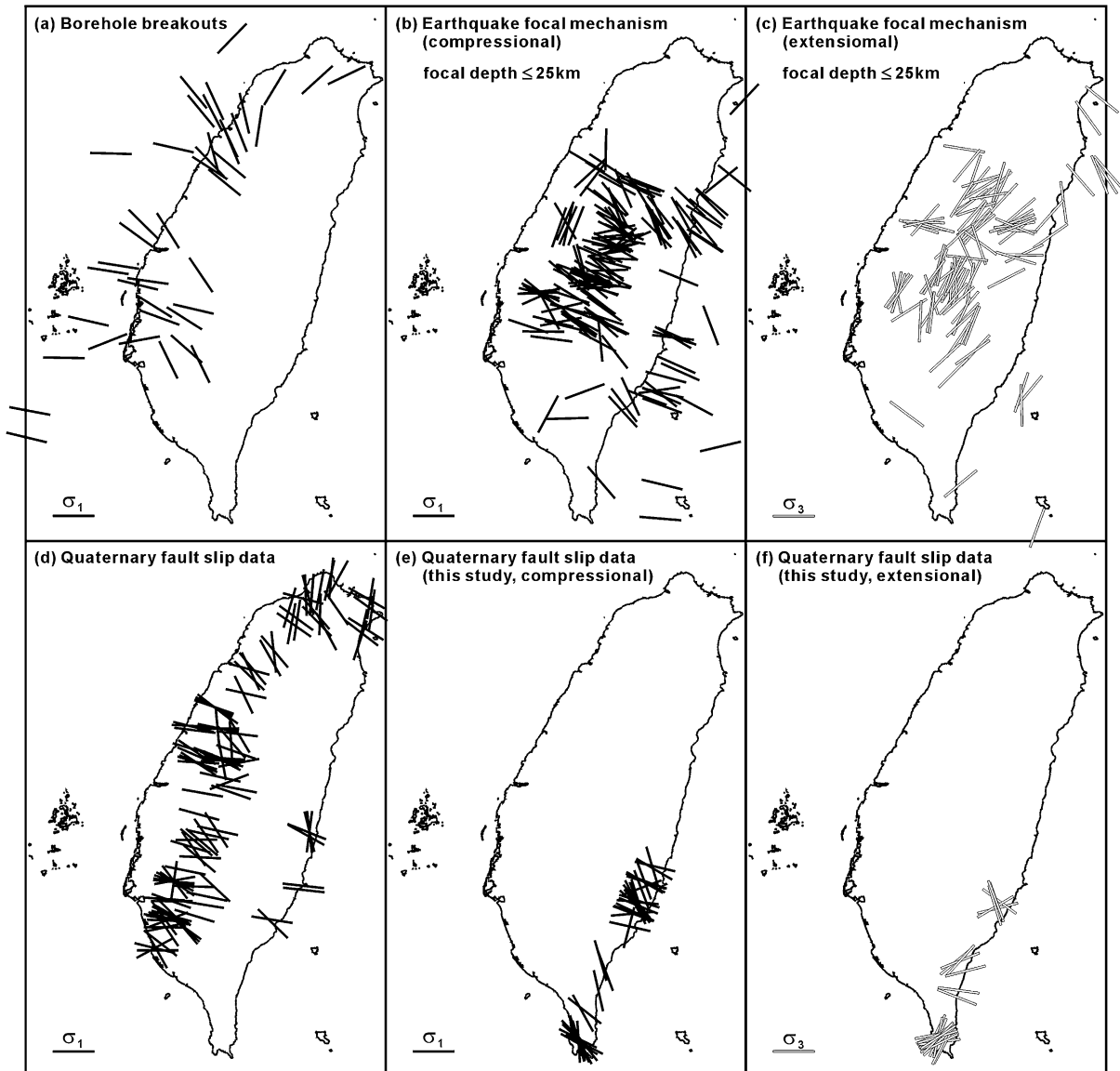
Fig. 5. Stress axes compiled from various tectonic sources. (a) Maximum horizontal stress orientation (σ_{hmax}) from borehole breakout data (after [26]). (b,c) *P* and *T* axes derived from the BATS/CMT focal mechanism solutions, earthquakes detected from 1995 to 2000. (d) Compressive paleostress related to Quaternary collision (reconstructed from fault slip data in Quaternary formations, after [33–37]). (e,f) Quaternary paleostress reconstructed from fault slip data in southeastern Taiwan.

Rather than carrying out extensive inversion of the focal mechanism data (e.g. [29,30]), we simply show the trends of the *P* and *T* axes where these axes have plunges less than 45°. It follows that a reverse-type earthquake is represented by a solid bar in Fig. 5b, a normal-type earthquake is rep-

resented by an open bar in Fig. 5c, whereas for a strike-slip-type earthquake there are bars in both Fig. 5b and Fig. 5c. The stress significance of the *P* and *T* axes is of course questionable, because these axes do not correspond to stress axes unless particular conditions are fulfilled. The stress ori-

entation would be better constrained with more elaborate graphical [31] or numerical methods [32]. However, as far as one simply aims at obtaining a rough picture of regional stress orientations, considering the orientations of *P* and *T* axes of focal mechanisms is acceptable in the very first approximation provided that many dip-slip-type focal mechanisms are present, which is the case. Not surprisingly, these *P* axes (Fig. 5b) and *T* axes (Fig. 5c) respectively trend approximately parallel and perpendicular to the average NW–SE direction of σ_{hmax} indicated by the borehole breakout analysis in western Taiwan (Fig. 5a).

The distribution of the Quaternary paleostresses also deserves consideration. It was studied in detail based on fault slip data analyses [33–37], as summarized in Fig. 5d in terms of the trends of compression (σ_1). Most of these studies concentrated on the western part of Taiwan. Some unpublished results have been added in Figs. 5e (σ_1 trends) and Figs. 5f (σ_3 trends), because they fill some gaps in the previously reconstructed pattern, especially in southern and southeastern Taiwan. The analysis of the fault slip data sets collected in the field involved inversion to obtain the stress tensors, according to methods described and discussed in previous papers [38,39]. Not only do the results shown in Fig. 5d–f confirm the importance of the NW–SE directed compression throughout Taiwan, but also they reveal a fan-shaped pattern of σ_1 trajectories. Effectively, WNW–ESE and NW–SE average trends of compression respectively prevail in southwestern and northwestern Taiwan (Fig. 5d).

To summarize, the stress results of various origins shown in Fig. 5 concur to highlight the importance of a compressive stress orientation that reflects the oblique indentation of the Luzon Arc into the Eurasian continental margin (Fig. 1). This compression approximately trends NW–SE, and does not markedly differ from the direction of plate convergence. In more detail, the perturbations of stress are far from being negligible, and involve a fan-shaped pattern that was described elsewhere (e.g. [33]) and is well accounted for by numerical modeling [7]. In the next section, we compare the tectonic information obtained from
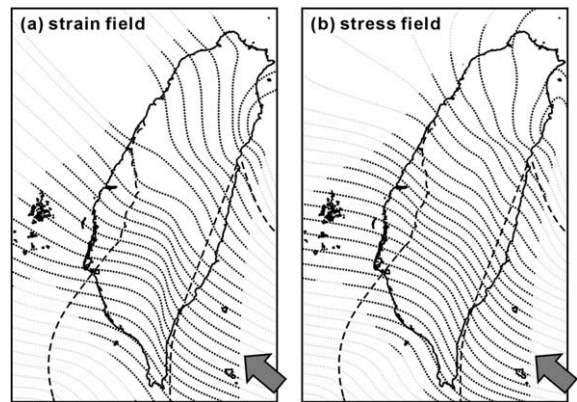

Fig. 6. Strain and stress trajectories for the Taiwan region. The trajectories derived from the extrapolation outside of the real measurements are faded. The gray arrow presents the direction of collision. (a) Strain field trajectories, this study. (b) Stress field trajectories, various sources (Fig. 5).

all the stress studies summarized in Fig. 5 with the rate of deformation field that we reconstructed from the GPS data.

5. Discussion

5.1. Trajectory maps of stress and strain fields in Taiwan

The two trajectory maps of Fig. 6 were reconstructed using a simple linear interpolation method [40]. The map of Fig. 6a refers to the GPS-based contraction trajectories (this paper). The map of Fig. 6b refers to the compression trajectories derived from all sources cited above. The first-order feature of both these maps is the fan-shaped trajectory pattern with a NW–SE trending axis, especially for northern and western Taiwan. Concerning the eastern Longitudinal Valley and the Costal Range, the trajectory trend is in good agreement with the direction of collision, as illustrated from both the stress and strain fields. Such a similarity might seem unexpected, because deformation rate and stress differ in principle. However, keeping in mind the small average amount of deformation per year (that is, between 10^{-8} and 10^{-5}), one remembers that the difference between stress and strain orientations is small when
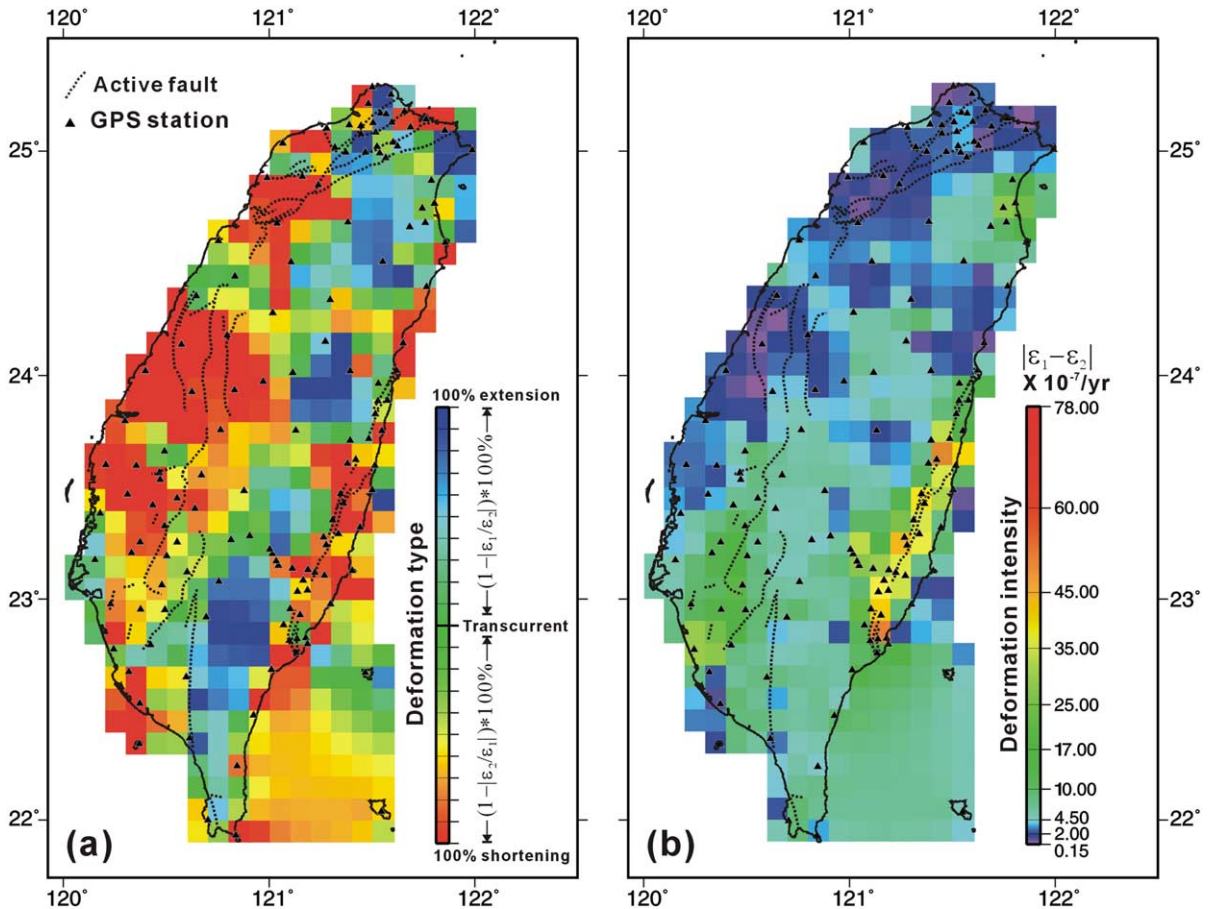
Fig. 7. Type and amplitude of the horizontal deformation of Taiwan, this study. The documented active faults are indicated in each sub-figure. (a) Deformation types, derived from the ratio of the extension and shortening components for each strain pair. (b) Differential strain, as the absolute difference between the two eigenvalues.

the deformation is minor and penetrative. For this reason, the resemblance between the two maps of Fig. 6 should not be considered surprising.

It is worth noting that the strain pattern refers to a 5-yr period (1990–1995), whereas the stress pattern is reconstructed from results that cover a variety of time spans, from a few years or decades (borehole breakouts and focal mechanisms) to about one million years (Quaternary paleostress data). However, the distribution obtained for the 1990–1995 period that belongs to the interseismic stage resembles the distribution obtained for longer periods that incorporate both the interseismic and coseismic stages, as Fig. 6 suggests. More accurately, this observation is supported by inversion analyses of the Chi-Chi earthquake sequence, which revealed coseismic and postseismic stress patterns that did not markedly differ from the preseismic stress pattern [30]. It is interesting to note that despite the well-known differences related to elastic strain–stress accumulation during interseismic periods and discharge during major seismic events, the deformation reconstructed over a limited time span (5 years, Fig. 6a) is representative of the permanent tectonic behavior of the collision zone (Fig. 6b), in terms of type and orientations. Nonetheless, this conclusion cannot extrapolate relative stress–strain magnitudes, which may dramatically vary among different seismic cycles.

5.2. Spatial distributions of deformation type and intensity

Based on the resultant strain rate field, we implemented two analyses to highlight the spatial distribution in terms of deformation type and intensity (Fig. 7). The resultant patterns show that the Taiwan orogeny includes zones with contrasting deformation modes and amounts. Fig. 7a summarizes the deformation of Taiwan with three principal types: shortening, extension, and transcurrent. We define the type of deformation from the ratio of contraction and extension for each pair of strain rates. A 100% extension implies that both strain rates correspond to extensive deformation, whereas a 100% contraction implies that both eigenvalues represent compressive deformation. The ideal transcurrent situation is defined by strain rates with equal absolute values but with opposite signs of deformation. We thus defined a complete scale of deformation types in the horizontal plane. Fig. 7a shows that extension dominates in the Central Range. Areas of extension may reflect major thickening near the collision boundary according to the bulldozer theory [41], or it may reflect body forces related to the negative buoyancy of the hot and weak Central Range lithosphere (e.g. [42]). In contrast, both the Coastal Range to the east and the foreland belt to western Taiwan present a deformation dominated by shortening. Likewise some significant sections separated by transcurrent mode are observed along the direction of Taiwan's main trunk (Fig. 7a).

Fig. 7b presents the deformation intensity, in terms of differential horizontal strains. Our study thus reveals a maximum intensity of differential deformation in the Longitudinal Valley, which is the suture zone (Fig. 7b). In western Taiwan, this map shows diffuse zones that resemble the pattern observed in Fig. 7a. It is noticeable that the coseismic rupture area of the 1999 Chi-Chi earthquake shows little deformation (Figs. 1 and 7b), and a considerable deformation exists north of this rupture area, which geographically corresponds with the Sanyi–Puli seismic zone (Figs. 4 and 7b). Fig. 7b also shows that a pattern of high deformation intensity in southwestern Taiwan

more or less overlaps with the presence of the major active faults, suggesting that the largest deformation usually takes place along the major existing structures.

Taking into account that these analyses are referred to the GPS data collected in an interseismic period, an area with little deformation deserves consideration in that it may reveal either a situation with low stress and little deformation, or a situation of increasing strain–stress accumulation. The occurrence of the Chi-Chi earthquake is apparently consequent on the latter. Looking at Fig. 7b, the epicentral and central rupture trace area of the Chi-Chi earthquake is consistent with a low deformation intensity, whose pattern is centered near 24°N, 120.7°E (central western Taiwan, dark blue and purple in Fig. 7b). In the neighboring east, a zone with low strain rates, extending from 23.5°N, 121.5°E to 24°N, 120.5°E, is observed to connect the Chi-Chi rupture area to the west and the Longitudinal Valley to the east. The orientation of this zone consists with the main contraction direction of Taiwan. In the Central Range, this zone cuts across the otherwise continuous belt-parallel domains where strike-slip type and normal-type deformations prevail (Fig. 7a).

The significance of this zone is certainly questionable because of both the poor records of vertical displacement data, which preclude accurate three-dimensional reconstruction of the deformation, and the small number of stations in the Central Range. However, from the seismological point of view, ongoing deformation with dominating contraction can accumulate efficient compressive energy during a certain period without significant stress drop, and may suddenly cause a great event like the Chi-Chi earthquake.

To summarize the results shown in Fig. 7a,b, the general pattern is that there is compressional high strain rate in the east (in particular SE), compressional low strain rate in the west, and extensional moderate strain rate in the middle of Taiwan (the Central Range). Among these great divisions, some northwest trending zones with compressive mode and low strain rates can also be delineated across the Central Range (Fig. 7a,b). Nevertheless, in the absence of stress infor-

mation it is still difficult to extrapolate the relationship between all these deformation features and the occurrence of large earthquakes. A good example of such ambiguity comes from the NW–SE elongated low-deformation area that extends from 24°N, 121.7°E to 25°N, 121°E in northern Taiwan (dark blue and purple in Fig. 7b). This zone shows a similar deformation feature as the one east of the Chi-Chi rupture area, while there are no large earthquakes documented for this area so far. One contrasting interpretation can be proposed depending on whether the compressive stress is accumulating on land in western Taiwan or dissipated offshore eastern Taiwan near 24°N, 122°E.

6. Conclusions

For a convergent system like Taiwan, our study shows that the stress field and strain rate fields reflect perceptively the collision mechanism. The maximum deformation is located along the lithologic suture zone – the Longitudinal Valley, in eastern Taiwan (Figs. 4 and 7b). In western Taiwan, the strain field reflects the accommodation of the ongoing lithospheric deformation within the seismogenic portion and exhibits zones with contrasting deformation modes and amounts in different geological settings. It can support the inference that the inherited structure in western Taiwan, for example the Peikang High, plays a role in redirecting the stress–strain orientation and influences the regional accumulation of compressive stresses.

In this article, the strain field derived from the GPS steady motion has been compared with the tectonic information provided by studies of borehole breakouts, earthquake focal mechanisms and fault slip data. This comparison reveals a very consistent pattern in terms of compressive orientations. Despite the short-term variations related to the earthquake cycle, which affect to a large extent the distribution of magnitudes and to a smaller extent the distribution of type and orientation, some major long-term features of the deformation field are well highlighted by the GPS surveys. This concept can provide useful insights

into temporal and spatial variations of strain, which is as a function of local heterogeneity and transition between interseismic and coseismic periods.

References

[1] F.T. Wu, Recent tectonics of Taiwan, J. Phys. Earth 26 (1978) S265–S299.

[2] Y.B. Tsai, Seismotectonics of Taiwan, Tectonophysics 125 (1986) 17–37.

[3] S.B. Yu, H.Y. Chen, L.C. Kuo, Velocity field of GPS stations in the Taiwan area, Tectonophysics 274 (1997) 41–59.

[4] C.C. Liu, S.B. Yu, Vertical crustal movements in eastern Taiwan and their tectonic implications, Tectonophysics 183 (1990) 111–119.

[5] J. Suppe, Geometry and kinematics of fault-bend folding,. J. Sci. 283 (1983) 684–721.

[6] L.S. Teng, Y. Wang, C.H. Tang, T.C. Huang, M.S. Yu, A. Ke, Tectonic aspects of the paleogene deposition basin of northern Taiwan, Proc. Geol. Soc. China 34 (1991) 313–336.

[7] J.C. Hu, S.B. Yu, J. Angelier, H.T. Chu, Active deformation of Taiwan from GPS measurements and numerical simulations, J. Geophys. Res. 106 (2001) 2265–2280.

[8] K.F. Ma, C.T. Lee, Y.B. Tsai, The Chi-Chi earthquake: large surface displacement on an inland thrust fault, EOS Trans. AGU 80 (1999) 605.

[9] C.S. Hou, T.C. Lia, L.Y. Fei, J.S. Wang, W.H. Chen, Highly accurate surveying in the study of the Chelungpu active fault-comparison of the data before and after the Chi-Chi Earthquake, Central Geological Survey (MOEA, Taipei) Spec. Publ. 12 (2000) 191–210.

[10] S.B. Yu, L.C. Kuo, Y.J. Hsu, H.H. Su, C.C. Liu, C.S. Hou, J.F. Lee, T.C. Lai, C.C. Liu, C.L. Liu, T.F. Tseng, C.S. Tsai, T.C. Shin, Pre-seismic deformation and coseis-

mic displacements associated with the 1999 Chi-Chi, Taiwan, Earthquake, Bull. Seism. Soc. Am. 91 (2001) 995–1012.

[11] T. Seno, The instantaneous rotation vector of the Philippine Sea plate relative to the Eurasian plate, Tectonophysics 42 (1977) 209–226.

[12] T. Seno, S. Stein, A.E. Gripp, A model for the motion of the Philippine Sea plate consistent with NUVEL-1 and geological data, J. Geophys. Res. 98 (1993) 17941–17948.

[13] K.M. Yang, H.H. Ting, J. Yuan, Structural styles and tectonic modes of Neogene extensional tectonics in southwestern Taiwan: implications for hydrocarbon exploration, Petrol. Geol. Taiwan 26 (1991) 1–31.

[14] A.T. Lin, A.B. Watts, Origin of the western Taiwan basin in orogenic loading and flexure of a rifted continental margin, J. Geophys. Res. 107 (2002) ETG2-1–ETG2-19.

[15] C.S. Ho, A synthesis of the geologic evolution of Taiwan, Tectonophysics 125 (1986) 1–16.

[16] J. Suppe, Imbricated structure of western foothills belt, south-central Taiwan, Petrol. Geol. Taiwan 17 (1980) 1–16.

[17] J. Angelier, H.C. Chu, J.C. Lee, J.C. Hu, Active faulting and earthquake hazard: The case study of the Chihshang fault, Taiwan, J. Geodyn. 29 (2000) 151–185.

[18] J.C. Lee, J. Angelier, H.T. Chu, J.C. Hu, F.S. Jeng, Continuous monitoring of an active fault in a plate suture zone a creepmeter study of the Chihshang Fault, eastern Taiwan, Tectonophysics 333 (2001) 219–240.

[19] S.B. Yu, L.C. Kuo, Present-day crustal motion along the Longitudinal Valley Fault, eastern Taiwan, Tectonophysics 333 (2001) 199–217.

[20] W.H.F. Smith, P. Wessel, Gridding with continuous curvature spines in tension, Geophysics 55 (1990) 293–305.

[21] J. Letouzey, M. Kimura, The Okinawa trough genesis, structure and evolution of the backarc basin developed in a continent, Mar. Petrol. Geol. 2 (1985) 111–130.

[22] Y.H. Yeh, C.H. Lin, S.W. Roecker, A study of upper crustal structures beneath northeastern Taiwan: possible evidence of the western extension of Okinawa trough, Proc. Geol. Soc. China 32 (1989) 139–156.

[23] B. Deffontaines, O. Lacombe, J. Angelier, H.C. Chu, F. Mouthereau, C.T. Lee, J. Deramond, J.F. Lee, M.S. Yu, P.M. Liew, Quaternary transfer faulting in the Taiwan Foothills: evidence from a multisource approach, Tectonophysics 274 (1997) 61–82.

[24] C.Y. Lu, J. Malavieille, Oblique convergence, indentation and rotation tectonics in the Taiwan Mountain belt: insight from experimental modeling, Earth Planet. Sci. Lett. 121 (1994) 477–494.

[25] O. Lacombe, F. Mouthereau, J. Angelier, B. Deffontaines, Structural, geodetic and seismological evidence for tectonic escape in SW Taiwan, Tectonophysics 333 (2001) 323–345.

[26] J. Suppe, C.T. Hu, Y.J. Chen, Present-day directions in western Taiwan inferred from borehole elongation, Petrol. Geol. Taiwan 21 (1985) 1–12.

[27] H. Kao, P.R. Jian, K.F. Ma, B.S. Huang, C.C. Liu, Moment-tensor inversion for offshore earthquakes east of Taiwan and their implications to regional collision, Geophys. Res. Lett. 25 (1998) 3619–3622.

[28] H. Kao, P.R. Jian, Source parameters of regional earthquakes in Taiwan July 1995-December 1996, TAO 10 (1999) 585–604.

[29] Y.H. Yeh, E. Barrier, J. Angelier, Stress tensor analysis in the Taiwan area from focal mechanisms of earthquakes, Tectonophysics 200 (1991) 267–280.

[30] H. Kao, J. Angelier, The Chi-Chi earthquake sequence, Taiwan: results from source parameters and stress tensor inversions, C.R. Acad. Sci. Paris, Sci. Terre Planet. 333 (2001) 65–80.

[31] J. Angelier, P. Mechler, Sur une methode graphique de recherche des contraintes principales également utilisables en tectonique et en séismologie: la méthode des diedres droits (Original title translated: A graphic method applied to the localization of principal stresses for fault tectonics and seismology; the right dihedral method), Bull. Soc. Geol. France 19 (1977) 1309–1318.

[32] J. Angelier, Stress tensor determination through inversion of double couple focal mechanisms of earthquakes without choice between nodal planes, C.R. Acad. Sci. Paris, Sci. Terre Planet. 334 (2002) 73–80.

[33] J. Angelier, E. Barrier, H.T. Chu, Plate collision and paleostress trajectories in a fold-thrust belt: The foothills of Taiwan, Tectonophysics 125 (1986) 161–178.

[34] E. Barrier, J. Angelier, Active collision in eastern Taiwan: the Coastal Range, Tectonophysics 125 (1986) 39–72.

[35] C.T. Lee, Methods of stress analysis and paleostress changes in northern Taiwan due to arc-continent collision, Ph.D. Thesis, National Taiwan University, Taipei (1986) 370 pp. (in Chinese).

[36] J. Angelier, F. Bergerat, H.C. Chu, T.Q. Lee, Tectonic analysis and the evolution of a curved collision belt: the Hsüehshan Range, northern Taiwan, Tectonophysics 183 (1990) 77–96.

[37] H.T. Chu, Néotectonique cassante et collision plio-quaternaire à Taiwan, Ph.D. thesis, Université P. et M. Curie, Paris, 1990, 292 pp.

[38] J. Angelier, From orientation to magnitudes in paleostress determinations using fault slip data, J. Struct. Geol. 11 (1989) 37–50.

[39] J. Angelier, Inversion of field data in fault tectonics to obtain the regional stress. III. A new rapid direct inversion method by analytical means, Geophys. J. Int. 103 (1990) 363–376.

40 J.C. Lee, J. Angelier, Paleostress trajectory maps based on the results of local determinations: the 'LISSAGE' program, Comput. Geosci. 20 (1994) 161–191.

[41] B.C. Burchfiel, L.H. Royden, North-south extension within the convergent Himalayan region, Geology 13 (1985) 679–682.

[42] C.H. Lin, Thermal modelling of continental subduction and exhumation constrained by heat flow and seismicity in Taiwan, Tectonophysics 324 (2000) 189–201.